

SMALL CRATERS ON THE METEOROID AND SPACE
DEBRIS IMPACT EXPERIMENT

Donald H. Humes
NASA Langley Research Center
Hampton, VA 23665-5225
Phone: 804/864-1484, Fax: 804/864-7730

10/15
1/3/77
36 P

SUMMARY

Examination of 9.34 m² of thick aluminum plates from the Long Duration Exposure Facility (LDEF) using a 25X microscope revealed 4341 craters that were 0.1 mm in diameter or larger. The largest was 4 mm in diameter. Most were roughly hemispherical with lips that were raised above the original plate surface. The crater diameter measured was the diameter at the top of the raised lips. There was a large variation in the number density of craters around the three-axis gravity-gradient stabilized spacecraft. A model of the near-Earth meteoroid environment is presented which uses a meteoroid size distribution based on the crater size distribution on the space end of the LDEF. An argument is made that nearly all the craters on the space end must have been caused by meteoroids and that very few could have been caused by man-made orbital debris. However, no chemical analysis of impactor residue that will distinguish between meteoroids and man-made debris is yet available. A small area (0.0447 m²) of one of the plates on the space end was scanned with a 200X microscope revealing 155 craters between 10 μm and 100 μm in diameter and 3 craters smaller than 10 μm. This data was used to extend the size distribution of meteoroids down to approximately 1 μm. New penetration equations developed by Alan Watts were used to relate crater dimensions to meteoroid size. The equations suggest that meteoroids must have a density near 2.5 g/cm³ to produce craters of the shape found on the LDEF. The near-Earth meteoroid model suggests that about 80 to 85 percent of the 100 μm to 1 mm diameter craters on the twelve peripheral rows of the LDEF were caused by meteoroids, leaving 15 to 20 percent to be caused by man-made orbital debris.

INTRODUCTION

For nearly six years, the Long Duration Exposure Facility orbited the Earth with 57 scientific experiments on board that were to be evaluated when the spacecraft was returned to the ground. There was no communication with the LDEF while it was in orbit. The Meteoroid and Space Debris Impact Experiment, designated S0001 by the LDEF Project Office, consisted of many thick aluminum plates distributed around the spacecraft to study the population, directionality, and chemical composition of meteoroids and man-made orbital debris. All the data will be obtained from examination of the craters left in the aluminum plates. In some places in the literature this experiment is referred to by a shortened title as the Space Debris Impact Experiment.

Meteoroids are small interplanetary particles that travel through our solar system undetected and whose encounter can only be treated statistically. They are natural particles that are in orbit about the sun. Meteoroids that pass near the Earth are drawn toward the Earth by its gravitational field and some strike spacecraft as they speed toward the atmosphere. Meteoroids have been considered a hazard to spacecraft since the beginning of space exploration. NASA has published models of the meteoroid environment near the Earth (ref.1) and in interplanetary space (ref.2), and a design criteria document for protection against meteoroids (ref.3). However, the interest in meteoroids is broader than the concern about the hazard they present to spacecraft. Meteoroids may include unaltered primal material whose composition and orbital paths are important clues to the origin and evolution of the solar system.

Space debris is the man-made material left in space as a result of our space activity. It ranges in size from microscopic fragments created during explosions in space to large spent rockets. Some man-made debris escapes the Earth's gravity but most is left in orbit about the Earth and is of concern as a potential hazard to spacecraft. Large pieces of debris are tracked and cataloged and possible collisions with the Space Transportation System (STS) orbiter are checked for each mission so that evasive measures can be taken if necessary. Small pieces cannot be tracked and their encounter, like that of meteoroids, must be treated statistically. NASA now has a model of the man-made orbital debris environment (ref.4) to be used in hazard analysis.

The LDEF maintained a three-axis gravity-gradient stable orientation, which provided a new level of sophistication in flight data on meteoroids and man-made debris. In previously obtained flight data in near-Earth space, see ref.1, the number of meteoroid impacts was obtained but the orientation of the impact site at the time of the impact was unknown. The number density of craters for the different fixed surface orientations on the LDEF provides a direct measurement of the degree to which the hazard to spacecraft is directional. The variation in the number density of craters with surface orientation depends on the orbital distribution of the particles. While the orbits of individual particles cannot be determined with this experiment, theoretical orbital distributions can be checked by seeing if they are in agreement with the crater distribution found on the LDEF.

Some aluminum plates donated to the LDEF Meteoroid and Debris Special Investigation Group (M&D SIG) by principal investigators of other LDEF experiments were examined and the results are included in this paper. Wayne Slep donated the aluminum base plates, sample holders and cover plates from his experiments (S0010 and AO134) on the only side of the LDEF from which the Meteoroid and Space Debris Impact Experiment plates were missing. His contribution is especially significant because that side of the LDEF received the greatest concentration of impact craters. William Berrios donated the aluminum thermal panels from both ends of the LDEF. The dummy plates that covered two unused experiment compartments on the Earth-facing end of the LDEF were also examined.

The research reported in this paper is a continuation of that presented in ref.5. There, craters with a diameter of 0.5 mm or greater, found in thick aluminum plates from all fourteen faces of the LDEF, were counted and measured, and a model of the near-Earth meteoroid environment, based on the magnitude of the crater density and its variation with location around the spacecraft, was presented. Here, the research is extended down to 0.1 mm craters, and for the

space end, down to 10 μm diameter craters. The new data is used to improve the near-Earth meteoroid environment model. Throughout this paper paragraphs can be found that were copied verbatim from ref.5 for completeness.

EXPERIMENTAL HARDWARE

The Meteoroid and Space Debris Impact Experiment exposed 26.29 m^2 of thick aluminum plates (4.8 mm thick) to the space environment. The location of the plates on the LDEF is shown in Fig.1. The plates were mounted on the bottom of 7.6 cm deep trays, except for the plates in Tray D6, which were mounted even with the top of the tray.

The nineteen peripheral trays that were totally dedicated to this experiment had two plates measuring 0.62 m by 0.95 m in each tray. The three peripheral trays that were shared with other experiments had two plates measuring 0.41 m by 0.95 m in each tray. These individual plates are identified by the tray location number and the relative position of the two plates in the tray. For example, the two plates in the tray in location F10 are identified as plates F10G and F10H, with F10G being the plate nearest the G-end or Earth-facing end of the LDEF. The three end trays each contained a single plate that was 0.72 m by 0.72 m.

In ref.5 the area of the Meteoroid and Space Debris Impact Experiment was mistakenly given as 26.32 m^2 . The 0.03 m^2 target on plate A6H, that was used as a berthing aid, shielded part of the plate. It was removed during de-integration and was not examined as part of this study.

The Meteoroid and Space Debris Impact Experiment plates were made of aluminum alloy 6061-T6. They had a thin oxide layer on both sides produced by chromic anodization and a coat of black paint on the back for spacecraft thermal control. The space-exposed side of the plates had a green or a pink tint due to the oxide layer produced during anodization. The plates from the Earth end and the space end (at locations G4, G8, and H5) were exceptions. They had the usual gray color of aluminum with only a natural oxide layer. They also were smoother than the plates from the peripheral trays. It would appear that they did not undergo the same sodium hydroxide cleaning and chromic anodization as the plates in the peripheral trays, even though records show that they were treated like the other plates.

The plates donated by Wayne Slemph were from his tray at location B9. They were anodized aluminum, 6061-T6, of various thicknesses from 1.6 mm to 6.4 mm. The plates that were studied and the identification numbers used for them are shown in Fig.2. Plate B9P5 was a large specimen holder under the B9P4 retainer plate, but only a small portion of it was exposed to the space environment. B9P1 and B9P5 were 6.4 mm thick, B9P4 and B9P6 were 2.1 mm thick, and B9P2 and B9P3 were 1.6 mm thick. Twenty-nine of the 32 clamps used to hold specimens on the plates were also examined. All the clamps were 2.2 mm thick aluminum 6061-T6. When the clamps were removed from the tray they were not individually identified and were mixed together with clamps from the back of the tray that had been used to hold control samples to the plates.

Then identification numbers ranging from B9P7 to B9P63 were assigned to the clamps. Later, the space-exposed clamps were identified by impact craters and contamination patterns.

The thermal panels donated by William Berrios covered the area around the edges of the two ends of the LDEF that was not being used for experiments. The twelve thermal panels on the space-facing end were assigned identification numbers H13 to H24, and those on the Earth-facing end, G13 to G24, by the LDEF M&D SIG (see Fig.1). Each thermal panel was bent to wrap around the corner of the spacecraft, exposing a small rectangular area along one of the spacecraft rows. The two surfaces of a thermal panel, with their orthogonal viewing directions, are considered as two separate plates in this paper. A symbol in parenthesis following the thermal panel identification number designates the orientation of the surface, (S) for a space-facing surface, (E) for an Earth-facing surface, and (R6) for a surface along Row 6, for example. The thermal panels were made of 1.6 mm thick aluminum (6061-T6) and had coatings for thermal control. Those on the space end were anodized to reflect sunlight and were painted black on the back. Those on the Earth end were plated with elemental nickel (nominally 15 μm thick) and then coated with black chrome (nominally 0.1 μm thick) to absorb sunlight reflected off the Earth. The back of the Earth end thermal panels were apparently masked during the plating process and were then painted black, except along the edges.

The two dummy plates on the Earth-facing end were anodized aluminum (6061-T6), 2.3 mm thick. Each plate had an area of 0.90 m². One was identified as G9 by the LDEF M&D SIG, and the other as G3.

LDEF MISSION

The LDEF was deployed by the STS-41C crew on April 7, 1984. It was initially placed in a near-circular orbit with an apogee of 480 km, a perigee of 474 km, and an inclination of 28.5 degrees. By the time it was recovered by the STS-32 crew on January 12, 1990, it had fallen to an altitude of 331 km.

It was intended for the longitudinal axis of the spacecraft to be aligned with its Earth-centered position vector and for the normal to the Row 9 trays to be aligned with the velocity vector. Post-flight analysis showed that the actual orientation had a misalignment of about eight degrees in yaw and one degree in pitch; see ref.6. As a result, the leading edge of the LDEF was between Row 9 and Row 10. The one degree pitch angle gave the space-facing end a slight view of the forward direction of flight.

DESCRIPTION OF CRATERS

The craters in aluminum on the LDEF look very much like craters produced with hypervelocity accelerators in the laboratory at impact speeds greater than 6 km/s. The craters are

generally round with lips that rise above the surface of the plate. The photograph in Fig.3 shows the top view of a crater on the F10H plate. This 4 mm diameter crater is the largest on any of the Meteoroid and Space Debris Impact Experiment plates and is the largest crater examined in this study.

Most of the craters are round and symmetric, which is surprising considering that the impacting particles were undoubtedly irregular in shape and must have struck at oblique angles. The cavity below the plate surface is usually nearly hemispherical. The typical shape of the craters is shown in Fig.4. Three dimensions are shown: the diameter at the top of the raised lips, the diameter at the plate surface, and the depth. The diameter at the plate surface is considered to be a more fundamental dimension than the diameter at the top of the raised lips, but it is more time-consuming to measure, so in this study the lip diameter is reported. The diameters shown in the figures and in the tables in this paper are all lip diameters.

The shape of the craters varies with crater size. Craters with a lip diameter of 0.5 mm or greater are usually very nearly hemispherical ($P/d_c = 0.5$) while smaller craters are usually deeper than hemispheres, with 100 μm craters having a depth about 0.56 times the diameter at the plate surface.

The shape of the craters was determined with a high-power microscope, typically 200X or greater. The very short depth of field of a high-power microscope is required to measure the depth of the crater and to measure the diameter at the plate surface. To obtain the crater shape data in Fig.4, the diameter at the top of the raised lips was also measured with the high-power microscope.

However, the scanning of the aluminum plates to obtain crater fluxes, for craters with a lip diameter of 100 μm or greater, was done with a low-power microscope, and a systematic difference of about 6 percent was found in the lip diameter measurements obtained with the low-power microscope and the high-power microscope, probably due to the effect that the difference in lighting had on the judgement of the location of the crest of the lips. The low-power microscope used an external ring light attached to the objective lens. The high-power microscope used light passing out of the objective lens for illumination. The lip diameters measured were about 6 percent greater when the high-power microscope was used.

Equations that relate crater size to projectile size, speed, density, impact angle and other properties use crater depth or crater diameter at the plate surface. The diameter at the top of the raised lips is never used. The equations, however, can be modified to calculate the crater lip diameter using the crater shape information in Fig.4, and that has been done in this paper when theoretical calculations were made to compare the near-Earth meteoroid model to the spacecraft data. The variation in crater shape with crater size for craters with a lip diameter less than 500 μm was estimated from the two cases shown in Fig.4.

There were no craters on any of the plates examined that penetrated through the entire thickness of the plate. The impact that created the largest crater on the Meteoroid and Space Debris Impact Experiment, the 4 mm crater on the F10H plate, produced a very short, raised dome on the

back of the 4.8 mm thick plate. The dome was less than 25 μm high. It is not known if it is just the black paint that delaminated and raised up or whether the aluminum plate is actually bulged.

The two thinnest donated plates from Row 9 had a total of four craters in the 1.6 mm thick aluminum that caused the back of the plates to bulge.

There was one near penetration of the 1.6 mm thick thermal panels. An impact that created a 1.02 mm deep crater on the portion of the G23 thermal panel that was along Row 10 caused spallation of aluminum from the back of the thermal panel.

There were ten impacts that caused a bulge in the back of the thermal panels. Most of the bulges occurred on the unpainted areas near the edges of the thermal panels. There were twelve impacts on the thermal panels that caused the black paint on the back to spall. Most of the paint spallation occurred without any detectable bulge in the aluminum.

NUMBER AND LOCATION OF CRATERS

A low-power (25X) microscope was used to scan 9.34 m² of aluminum plates that came from all fourteen faces of the LDEF in order to obtain the number density of craters with a lip diameter of 0.1 mm or greater on each face. While scanning the plates from the space-facing end, special attention was taken, and an attempt was made to find all craters with a lip diameter of 60 μm or greater. The survey was probably complete for 80 μm diameter craters and larger but was probably incomplete for 60 μm craters. A total of 4824 craters were found with the low-power microscope, 4341 of which had a lip diameter of 0.1 mm or greater and 483 of which were craters smaller than 0.1 mm from the space-facing end.

A 0.0447 m² area in the center of the space-facing plate from Tray H5 was scanned a second time, using a high-power (200X) microscope to obtain the number density of craters with a lip diameter of 10 μm or greater. A total of 138 craters with lip diameters between 10 μm and 60 μm were found along with the 51 craters with a lip diameter of 60 μm or greater that had been previously found during the low-power (25X) microscope survey. Three craters smaller than 10 μm were also found. The survey was probably complete for craters with a lip diameter of 20 μm or greater but some craters between 10 μm and 20 μm may have been missed.

In addition, the entire 26.29 m² of the Meteoroid and Space Debris Impact Experiment and 15.84 m² of plates donated to the M&D SIG were reexamined using a 12.5X microscope to obtain the number density of craters with a lip diameter of 0.5 mm and greater on all fourteen faces of the LDEF. The number densities differ slightly from those reported in ref.5. The fluxes presented in this paper are slightly higher for all the faces except for the space end and the trailing edge (Row 3) where they are lower, and for Row 9 and Row 10 where they are the same. A total of 965 craters with a lip diameter of 0.5 mm or greater were found on the 42.13 m² examined.

The distribution around the LDEF of the 5678 craters with a lip diameter of 10 μm or greater is given in Table I and Table II. The orientation of the plates on the sides of the LDEF is given by the angle between the spacecraft velocity vector and the normal to the plate surface. The plates on each face are grouped together because the flux should be constant on any face from both meteoroids and man-made orbital debris. The area of the plates given is the actual area. No correction has been made for the shielding that occurs for the plates that were mounted on the bottom of the 7.6 cm deep trays.

The variation in the cumulative crater flux on the twelve peripheral rows of the LDEF is shown in Figs.5, 6 and 7 for various threshold crater sizes as a function of the surface orientation. The cumulative crater flux is the number density of craters of a given threshold size or larger divided by the duration of the mission. The flux is greatest at the front of the spacecraft for all size craters and decreases smoothly toward the back, except for the plates nearest the trailing edge where the flux increases again for all but the smallest craters. The row with the minimum measured crater flux varied with crater size.

The error bars, which are the 90 percent confidence limits calculated using the chi-squared distribution function in the manner suggested in ref.7, are appreciable because of the small number of craters, especially near the back of the LDEF. It may be that the increase in crater flux measured near the trailing edge for large craters is just a statistical variation.

The data points in Figs.5, 6 and 7 are alternately from the southern side and northern side of the spacecraft. The smoothness of the data shows that there is a north/south symmetry in the particulate environment in the size range considered in this paper.

The cumulative crater flux on the two ends of the LDEF is shown in Fig.8 for craters with a threshold lip diameter between 0.1 mm and 1 mm. The flux on the space-facing end is 30 to 60 times the flux on the Earth-facing end in that size range.

The cumulative crater flux on the space-facing end, extended down to a threshold lip diameter of 10 μm , is shown in Fig.9. The slope between adjacent data points gets continuously flatter as smaller size craters are considered. This suggests that there may be a lower limit to the size of the meteoroids, i.e., a cutoff in the size distribution of meteoroids.

The data points in Figs.5,6,7 and 8 are the average flux for each face. In most cases, all of the plates on the same face give the same flux within the 90 percent confidence limits. One of the exceptions is the variation in flux between plates B9P2 and B9P4 which were side-by-side on the leading edge and differed by a factor of 1.3 in the flux of craters with a lip diameter of 0.1 mm or greater. With the number of craters of that size found on these two plates (400 total), we can be 90 percent confident that they were not exposed to the same environment. Of course, there is about a 10 percent chance that they were. The most likely explanation for the discrepancy is that there was a slight difference in the properties of the plates, or the oxide layer on the surface, that affected the formation of the crater lips.

PREVIOUS MODELS OF THE PARTICULATE ENVIRONMENTS

In the first paper on the results of this experiment (ref.5), data on large craters was presented on craters with a lip diameter of 0.5 mm or larger. The number of those craters and their distribution around the spacecraft suggested that more than 80 percent had been caused by meteoroids and less than 20 percent by man-made orbital debris. A new model of the near-Earth meteoroid environment was presented in ref.5 based on the assumption that all the large craters were caused by meteoroids. The man-made orbital debris model of Kessler (ref.4), which predicted that man-made debris was only a minor component in this size range, was seen to be plausible and no modifications to it were suggested.

Knowing the distribution of these large craters around the three-axis gravity-gradient stabilized LDEF provided the information needed to bring a new level of sophistication to the modelling of the near-Earth meteoroid environment. Proposed speed distributions and directionality distributions of meteoroids could be checked by comparing the variation in the number density of craters around the spacecraft suggested by these distributions, to the LDEF data thought to be primarily from meteoroids. Of the four speed distributions studied, the distributions of Erickson (ref.8) and Kessler (ref.9), which are essentially identical to each other, were found to provide the best agreement with the LDEF data. The directionality distribution of meteoroids relative to the Earth was biased toward the zenith in that model, rather than being random, in order to agree with the larger than expected flux seen on the space-facing end of the LDEF.

The new model of the near-Earth meteoroid environment presented in ref.5 is discussed in detail. In it meteoroids were assumed to have five properties: (1) a population in the near-Earth space expressed in terms of spatial density or number per unit volume, (2) a size distribution, (3) a speed distribution, (4) a direction of motion distribution with respect to the Earth, and (5) a mass density. It was assumed that the size distribution, speed distribution and directionality are independent of each other. The mass and size of the Earth affect the meteoroid environment and appear in that model in the form of (1) the gravitational focusing factor, which expresses the degree to which the impact flux tends to be enhanced by the Earth's gravitational field as the Earth is approached, and (2) Earth shielding, which tends to decrease the impact flux as the Earth is approached. Also, the equations used to relate meteoroid properties to impact damage were included as an essential part of the model.

However, when the near-Earth meteoroid environment model in ref. 5 is used to predict the flux of small meteoroid craters on the LDEF, it gives values that are higher than the measured crater flux, for every face, being about a factor of 1.4 higher for 100 μm diameter craters. Apparently, the size distribution of meteoroids in that model, which was obtained from the NASA near-Earth meteoroid model in ref.1, is wrong, having too many small meteoroids. Modifications to that near-Earth meteoroid environment model to correct that discrepancy are discussed in the following section of this paper.

The author of this paper has made no attempt to model the man-made orbital debris environment even though a comparison of the LDEF data and the modified near-Earth meteoroid

environment model in the following section of this paper suggests that the man-made orbital debris model of Kessler (ref. 4) is not accurate. There may be more man-made debris than predicted by Kessler (ref. 4) and its orbital distribution may be different.

MODIFIED MODEL OF THE NEAR-EARTH METEOROID ENVIRONMENT

Modifications to the near-Earth meteoroid environment model in ref.5 that bring it into agreement with the new data on small craters found on the LDEF are discussed in this section. It was the size distribution of meteoroids in the previous model that needed changing, but several other components of the model were changed as well. A new set of penetration equations developed by Watts (ref.10) from a more fundamental, physics-based analysis than those in ref.5 are used. The structure of the previous model is retained, i.e., the same properties of the meteoroid environment and the Earth are used and their relationship to each other is the same.

Approach

There are two components to the particulate environment near the Earth: meteoroids and man-made orbital debris. Chemical analysis is not yet available to determine which of the craters examined in this study were caused by meteoroids and which were caused by man-made debris. But in order to model the meteoroid environment, it is desirable to isolate the meteoroid craters from the man-made debris craters. That has been done on the space-facing end of the LDEF simply due to its orientation.

The crater flux on the space-facing end was 30 to 60 times the flux on the Earth-facing end for craters in the 0.1 mm to 1 mm size range (Fig.8). This shows that essentially all the craters on the space-facing end, in this size range, were caused by meteoroids. Very few, 2 to 3 percent, could have been caused by man-made orbital debris because the orbital debris would produce about the same crater flux on both ends of the LDEF. If the longitudinal axis of the LDEF had been aligned with its geocentric position vector, then Earth-orbiting particles would have the same relative speed and same impact angle when approaching the Earth-facing end from below as they would have when approaching the space-facing end from above, and the flux on both ends would be the same. This argument is not valid if the particles are very near the end of their orbital lifetime and their orbits are decaying rapidly. Then the particles would produce a greater flux on the space-facing end. But it is assumed here that the man-made orbital debris particles encountered by the LDEF in the size range needed to make 100 μm to 1 mm diameter craters were more permanent members of the orbital debris environment.

The longitudinal axis of the LDEF, however, was not exactly aligned with its position vector. The spacecraft was pitched forward about 1 degree so that the space-facing end had a slight view of the forward direction. This would tend to increase the flux on the space-facing end and

decrease the flux on the Earth-facing end, which was facing slightly backwards. This, however, did not account for any significant part of the factor of 30 to 60 difference in the flux on the two ends. The crater flux on the space-facing end was about the same for the H5 plate as it was for the thermal panels, even though the H5 plate was at the bottom of a 7.6 cm deep tray and the thermal panels were flush with the end of the LDEF. The recessed location of the H5 plate eliminated about 5 degrees from its field of view with little affect on the flux, so the 1 degree forward pitch of the LDEF could not have made a significant difference in the fluxes on the two ends. Therefore, we can assume that essentially all the craters on the space-facing end in the 0.1 mm to 1 mm size range were caused by meteoroids.

The size distribution of meteoroids can be determined from the size distribution of the craters on the space-facing end of the LDEF. The approach taken here to correct the size distribution of meteoroids in the model was to test various candidate meteoroid size distributions in the near-Earth meteoroid environment model from ref.5 and select the one that agreed best with the size distribution of craters on the space-facing end of the LDEF. The spatial density that gave the proper crater flux was determined at the same time.

Then the crater flux on the other faces of the LDEF, from meteoroids alone, was calculated. The difference between the calculated meteoroid flux and the greater measured flux would be assumed to be caused by man-made orbital debris. But before that was done, several other modifications were made to the model from ref.5. Independent reevaluations of all the other components of the model lead to changes in the directionality and mass density of meteoroids, to the gravitational effect of the Earth on meteoroids, and to the set of equations used to relate meteoroid properties to impact damage. The speed distribution of meteoroids and the height of the Earth's atmosphere (165 km) were not changed.

The following sections describe the components of the modified near-Earth meteoroid environment model.

Directionality

The directional distribution of meteoroids is the distribution of directions from which meteoroids would approach a stationary spacecraft. A distribution that was biased toward the zenith, rather than being random, was suggested in ref.5 to agree with the larger than expected relative flux on the space-facing end of the LDEF. New data from the examination of the thermal panels from the space-facing end, included in this paper, increased the area of the space-facing end examined from the 1.15 m² reported in ref.5 to 5.48 m², and the average flux of craters with a lip diameter of 0.5 mm or greater dropped from the $2.0 \times 10^{-7} \text{ m}^{-2}\text{s}^{-1}$ reported in ref.5 to $1.6 \times 10^{-7} \text{ m}^{-2}\text{s}^{-1}$. The data now available on the relative flux of craters with a lip diameter of 0.5 mm or greater on all the fourteen sides of the LDEF is consistent with a random directionality. As discussed in ref. 5, there is some theoretical basis for the random directionality of meteoroids with respect to stationary spacecraft, and so a random directionality is used in the modified near-Earth meteoroid environment model.

Speed Distribution

Four speed distributions of meteors published by astronomers were examined in ref.5 and the distributions of Erickson (ref.8) and Kessler (ref.9), which are essentially identical, provided the best agreement with the variation around the LDEF in the flux of craters with a lip diameter of 0.5 mm or greater. The reexamination of the plates studied in ref.5, and the inclusion of some additional plates in this paper, has resulted in slight changes in the relative flux of craters with a lip diameter of 0.5 mm or greater on the twelve peripheral rows of the LDEF, but the speed distributions of Erickson and Kessler still provide the best agreement and are used in the modified near-Earth meteoroid environment model.

A mathematical description of the Erickson and Kessler speed distributions is given by Zook (ref.11) as

$$f_{\phi}(V) = 0.112 \quad 11.1 \leq V < 16.3 \text{ km/s}$$

$$f_{\phi}(V) = 3.328 \times 10^5 V^{-5.34} \quad 16.3 \leq V < 55.0 \text{ km/s}$$

$$f_{\phi}(V) = 1.695 \times 10^{-4} \quad 55.0 \leq V < 72.2 \text{ km/s}$$

where $f_{\phi}(V)$ is the probability density for meteoroids entering the atmosphere with speed V , in km/s. This is actually the speed distribution of meteors in the Earth's atmosphere, corrected to a constant mass, while the model requires the speed distribution of meteoroids in space. The method of converting the speed distribution of meteors to the speed distribution of meteoroids in space is discussed in ref.5.

Gravitational Focusing

The flux of meteoroids on a spacecraft is enhanced by gravitational focusing, so that the closer the spacecraft is to the Earth, the greater the meteoroid flux tends to be. In this modified model, as in ref.5 and ref.2, the flux on a spacecraft is calculated first, ignoring gravitational focusing, and then that flux is multiplied by the gravitational enhancement factor, G , which for the Erickson (ref.8) or Kessler (ref.9) speed distribution is, according to Kessler (ref.9)

$$G = 1 + (r_e/r)$$

where r_e is the radius of the Earth and r is the distance of the spacecraft from the center of the

Earth. The expression for the gravitational enhancement factor, G, used in ref.5 actually applies to the speed distribution of meteoroids given in ref.1, and was mistakenly applied to the speed distributions of Erickson and Kessler in ref.5.

Earth's Atmosphere

While meteoroids have been assumed to approach a stationary spacecraft randomly from all directions, the Earth and its atmosphere shield the spacecraft from some of those meteoroids. In this modified model of the near-Earth meteoroid environment, as in ref.5, the Earth's atmosphere is assumed to extend to an altitude of 165 km. It is assumed that all meteoroids entering the atmosphere are destroyed.

Penetration Equations

Recently, Watts (ref.10) developed, from fundamental physics-based analysis, equations for the diameter of a crater and for the depth of a crater that a projectile would produce in a target as a function of the projectile and target properties. These two equations were developed independently, recognizing the differences in the stress history near the surface of a target and deep within the target. Watts also developed an equation for the thickness of material that a projectile can penetrate. These three equations have been adopted as an integral part of the modified near-Earth meteoroid environment model.

The Watts equation for the diameter of a crater at the surface of a target, d_c , is

$$d_c/d_p = 1.0857 F (\rho_p/\rho_t)^{0.2857} (\rho_t/Y_t)^{0.2857} (c_t/c_p)^{0.2857} (u_o \cos \theta)^{0.5714} / (1 + (\rho_p/\rho_t)^{1/2})^{0.5714}$$

where d_p is the diameter of the projectile, ρ_p is the density of the projectile material, ρ_t is the density of the target material, c_t is the speed of sound in the target, c_p is the speed of sound in the projectile, Y_t is the yield strength of the target material, u_o is the impact speed, θ is the impact angle measured from the normal to the target surface, and the scaling factor, F, is

$$F = 1 / (1 + (2\Delta/d_c)^{1/2})^N$$

where N is assumed to be 1/3 by Watts (ref.10) for aluminum 6061-T6 targets and is assumed to be 1/3 for all target materials in this paper, and Δ is a target material "grain size" parameter given by

$$\Delta = \pi G_t \gamma_s / Y_t^2$$

where G_t is the target material shear modulus, and γ_s is the target material surface energy per unit area for opening cracks. The “grain size” parameter, Δ , is not easy to obtain for all materials because γ_s is not often quoted. Watts suggests that Δ is about 50 μm for aluminum 6061-T6. The speed of sound in the meteoroid material (c_p) is not known and undoubtedly varies from particle to particle, but has been assumed to be 5 km/s in this paper.

The Watts equation for the depth of a crater, P , is

$$P/d_p = F (1/4)(4/3)^{1/3} (\rho_p/\rho_t)^{1/3} (\rho_t/Y_t)^{1/3} \{ (c_{ot} + s(u_o \cos\theta - u_{t,crit}) / (1 + (\rho_t/\rho_p)^{1/2})) (u_o \cos\theta - u_{t,crit}) \}^{1/3}$$

where c_{ot} is the speed of sound in the target when it is unstressed (c_t), s is $(1+\Gamma)/2$ where Γ is the Gruneisen parameter, and $u_{t,crit}$ is the critical impact speed for the target material above which the equation applies and is given by

$$u_{t,crit} = (2Y_t/\rho_p)^{1/2} (1 + (\rho_p/\rho_t)^{1/2}).$$

There is a critical impact speed for the projectile material also, $u_{p,crit}$, that must be exceeded for the penetration equation to apply. That is,

$$u_{p,crit} = (2Y_p/\rho_p)^{1/2} (1 + (\rho_p/\rho_t)^{1/2})$$

where Y_p is the yield strength of the projectile material. Y_p is not known for meteoroid material and undoubtedly varies from particle to particle, but if meteoroids have less strength than the target material then the target material will determine the critical impact speed. For the targets considered in this paper, that is assumed to be the case, and that probably is the case for most spacecraft materials. The critical impact speed, $u_{t,crit}$, is modest, less than 1 km/s for aluminum targets being struck by meteoroids or man-made orbital debris, so the equation is applicable to nearly all of the impacts on a spacecraft.

The Watts equation for the thickness of material a projectile can completely penetrate, T , is

$$T/d_p = F (1/8)(4/3)^{1/3} (\rho_p/\rho_t)^{1/3} (\rho_t/Y_t)^{1/3} \{ (c_{ot} + s(u_o \cos\theta - u_{t,crit}) / (1 + (\rho_t/\rho_p)^{1/2})) (u_o \cos\theta - u_{t,crit}) \}^{1/3} \\ + F(1/4) \{ \rho_p (u_o \cos\theta)^2 / (2\sigma_s (1 + (\rho_p/\rho_t)^{1/2})^2) \}^{1/N}$$

where a value of 2 is suggested for N by Watts in ref.10 and where σ_s is the ultimate strength of

the target material. The material properties of the target needed in these equations is given in Table III for three aluminum alloys.

Density

The crater size equations of Watts (ref.10) can be used to calculate the ratio of crater depth to crater diameter (P/d_c). A projectile density near 2.5 g/cm^3 is needed to obtain the depth-to-diameter ratios of 0.50 to 0.56 seen in the aluminum 6061-T6 plates on the LDEF, and that density has been assumed for meteoroids in the modified meteoroid model. The meteoroid density of 0.5 g/cm^3 used in ref.5 and in the NASA near-Earth meteoroid environment model (ref.1) would give depth-to-diameter ratios near 0.24.

Size Distribution and Spatial Density

With the modifications just described fixed, various meteoroid size distributions were tested in the near-Earth meteoroid model to see how well they predicted the crater size distribution on the space-facing end of the LDEF, which is assumed to be almost entirely from meteoroids. The results for three meteoroid size distributions are shown in Fig.10. The spatial density was adjusted to force all three curves to go through the LDEF data point for craters with a lip diameter of 0.5 mm or greater. The calculations were for plates that were flush with the end of the LDEF, like the thermal panels.

The size distribution from NASA SP-8013 (ref.1) predicts a flux of 0.1 mm diameter and larger craters that is about a factor of 1.1 higher than the measured flux on the LDEF. That is much less than the factor of 1.4 that prompted the rejection of that size distribution for use in the near-Earth meteoroid environment model in ref.5. The other modifications made to the model have improved the prediction of the flux of small craters making the selection of a new meteoroid size distribution less important for predictions in that size range. Changing the density of meteoroids from 0.5 g/cm^3 to 2.5 g/cm^3 probably had the greatest effect because in the penetration equations of Watts used in this paper, and in those used in ref.5, high density projectiles are predicted to create larger craters than low-density projectiles of the same mass. The change in meteoroid density caused a shift in the calculated mass of meteoroids responsible for the craters left on the LDEF. This shift, while improving the predictions for small craters, will cause the flux of large craters to be overestimated. That can be seen in Fig.10 for 1 mm and larger craters. The size distribution from SP-8013 is still found to be inaccurate.

The meteoroid size distribution of Grün (ref.12) agrees fairly well with the LDEF data in the flux of 0.1 mm to 0.5 mm diameter craters on the space end of the LDEF. It appears that the Grün size distribution also was based on the assumption that meteoroids had a density of 0.5 g/cm^3 . If the Grün curve were shifted, it would fit the data very well. But as it is, when used

with a meteoroid density of 2.5 g/cm^3 , it will overestimate the number of large craters created in a spacecraft, as seen in the 1 mm and greater diameter craters.

A new meteoroid size distribution is proposed that provides excellent agreement with the LDEF data, not only in the 0.1 mm to 1 mm diameter crater range, but also for craters between $10 \text{ }\mu\text{m}$ and 0.1 mm. It is not known if all the small craters on the space-facing end, $10 \text{ }\mu\text{m}$ to 0.1 mm, were caused by meteoroids or whether a significant fraction were caused by man-made orbital debris. The flux of these very small craters has not been measured on the Earth-facing plates so an argument based on the space end to Earth end ratio cannot be made. But it is assumed here that essentially all the small craters on the space end also were caused by meteoroids. If that assumption is incorrect the modified near-Earth meteoroid environment model will overestimate the flux of small craters caused by meteoroids on a spacecraft.

The proposed size distribution of meteoroids and their spatial density, S , in m^{-3} is

$$\log_{10} S = -8.362 \qquad m < 1.31 \times 10^{-12} \text{ g}$$

$$\log_{10} S = -18.251 - 1.664 \log_{10} m - 0.070 (\log_{10} m)^2$$

$$\log_{10} S = -18.188 - 1.213 \log_{10} m \qquad m > 5.00 \times 10^{-7} \text{ g}$$

where m is the meteoroid mass, in g.

TESTING THE MODEL

The model of the near-Earth meteoroid environment was then tested against three other sets of data: (1) the crater flux on the peripheral rows and on the Earth-facing end of the LDEF, (2) the crater flux in the aluminum louvers from the Solar Max spacecraft, and (3) the penetration flux through thin sheets of material on the Explorer 16, Explorer 23, and the three Pegasus spacecraft.

The meteoroid crater flux calculated for the twelve peripheral rows of the LDEF must match the measured fluxes if man-made orbital debris is not a significant component of the particulate environment in this size range, or be less than the measured flux if man-made debris is a significant component. If the calculated flux exceeds the measured flux, then the model is inaccurate and must be rejected. Likewise, for the Solar Max crater data, the calculated meteoroid crater flux must agree with or be less than the measured crater flux. The penetration flux data from the Explorer 16, Explorer 23, and the three Pegasus satellites was obtained in the 1960s when man-made orbital debris was, presumably, not significant, so the meteoroid model should match the fluxes measured.

Comparison With Other LDEF Crater Data

The calculated cumulative meteoroid crater flux on the twelve peripheral rows of the LDEF is compared with the measured flux in Figs.11,12, and 13 for craters with a threshold lip diameter of 0.1 mm, 0.2 mm, 0.3 mm, 0.5 mm and 1 mm. The calculation is for plates at the bottom of 7.6 cm deep trays taking into account the shielding provided by the tray walls. The calculated meteoroid crater flux is, in general, about 80 to 85 percent of the measured crater flux, suggesting that 15 to 20 percent of the craters in these size ranges were caused by man-made orbital debris.

The calculated cumulative meteoroid crater flux for the Earth end is compared to the measured flux in Fig.14 for plates that are flush with the end on the LDEF. The calculated meteoroid crater flux agrees with the measured crater flux within the 90 percent confidence limits, suggesting that most of the craters on the Earth end in the 0.1 mm to 1mm diameter range were caused by meteoroids.

The model passes the first test; it does not predict more craters on the peripheral rows and the Earth end of the LDEF than were actually found. It predicts what would seem to be a reasonable fraction of the crater flux measured.

Comparison With Solar Max Crater Data

The calculated cumulative crater flux for meteoroids striking the aluminum louvers on the Solar Max spacecraft is shown in Fig.15 along with the data obtained from examination of the louvers after they were returned to the Earth (ref.13). The data is also presented in Table IV.

The properties of the 1145-H19 aluminum alloy used to make the louvers are listed in Table III. The value of the "grain size" parameter, Δ , is not known so the results obtained using various values of Δ are presented in Fig.15.

Following the suggestion in ref.13, the Solar Max louvers were assumed to have been randomly oriented with respect to the Earth and to have been significantly shielded by other spacecraft components so that the measured flux was only 71 percent of that which an unshielded plate would experience. It was the lip diameter that was measured in ref.13 and so the theoretical crater diameter equation was converted to predict the lip diameter. For this conversion it was assumed that the craters in the 1145-H19 aluminum alloy were the same shape as those in the 6061-T6 aluminum alloy. In Fig.15, both the calculated fluxes and the Solar Max data are for an unshielded plate.

Watts suggests in ref.10 that Δ for some aluminum is about 50 μm . Unless the uncertainties in the assumptions account for the lack of agreement between the $\Delta = 50 \mu\text{m}$ calculation and the data (and that is quite possible), it appears the "grain-size" parameter, Δ , for the

1145-H19 aluminum alloy is greater than that for the 6061-T6 aluminum alloy, being between 200 μm and 500 μm . The calculated meteoroid flux, using $\Delta = 200 \mu\text{m}$, falls about 10 percent below the measured flux, and using $\Delta = 500 \mu\text{m}$, falls about 20 percent below the measured flux. It is estimated in ref.14 from chemical analysis of impactor residue found in many of the large penetration holes in the louvers (180 μm to 820 μm in diameter), that about 85 percent of the holes were caused by meteoroids and 15 percent by man-made orbital debris.

The accuracy of the model cannot be strictly evaluated by comparing it with the Solar Max data because of uncertainties about the louver material properties and the shape of the craters, but the model seems to be fairly accurate.

Comparison With Early Penetration Detector Experiments

In the 1960s, penetration detectors were flown in low-Earth orbit aboard Explorer 16, Explorer 23, and the three Pegasus satellites to measure the frequency with which meteoroids would completely penetrate thin sheets of material. This was not data on craters in a thick plate, but on perforation through a thin sheet. Explorer 16 used pressurized cells with a thin beryllium copper wall, either 25 μm thick or 51 μm thick. On Explorer 23, pressurized cells of 25 μm and 51 μm thick stainless steel were used. The detectors on the Pegasus spacecraft were capacitors with a 38 μm , 200 μm or 400 μm thick aluminum penetration plate backed by a 13 μm thick mylar dielectric and a rear capacitor plate. The detector plate was aluminum alloy 2024-T3 for the two thicker detectors and aluminum alloy 1100 for the thinnest detector. The meteoroid penetration fluxes measured by these spacecraft (refs.7,15) are presented in Table V and are plotted in Fig.16 as a function of detector thickness. No adjustment has been made to account for differences in the detector material. The actual detector thickness is plotted. The solid (filled in) data points are for the detectors that were made of aluminum. The flux plotted is the flux for an unshielded plate calculated using the transmission factors in Table V. The data from the three Pegasus satellites has been combined as suggested by Naumann (ref.15).

Data from the Solar Max spacecraft on the penetration flux through 50 μm kapton, 75 μm kapton, and the 125 μm thick aluminum louvers (ref.13), while not 1960s data, is also shown in Fig.16, and is presented in more detail in Table V.

The curve in Fig.16 is the calculated meteoroid penetration flux for aluminum 2024-T3 detectors that are randomly oriented with respect to the Earth, in a circular orbit at an altitude of 700 km, and that are not shielded by other spacecraft components. A value of 50 μm was assumed for the "grain size" parameter, Δ .

The model prediction is in excellent agreement with the data. The model curve agrees with the thick aluminum detector data, is above the Explorer 16 and Explorer 23 data for materials expected to be more resistant to penetration than aluminum, and is below the Solar Max data for kapton which is expected to be less resistant to penetration than aluminum. The only data point that seems to be out of place is that for the thin aluminum detector on Pegasus.

The way the Solar Max aluminum louver data falls in line with the Pegasus data suggests that the penetrations through the louvers were nearly all caused by meteoroids, just as the chemical analysis confirmed (ref.14). It also suggests that the meteoroid environment did not change significantly from the mid 1960's to the early 1980's.

DISCUSSION

Several improvements to the near-Earth meteoroid environment model from ref.5 have been presented in this paper. The use of the penetration equations developed by Alan Watts and their implication that meteoroid densities must be near 2.5 g/cm^3 instead of the previously assumed value of 0.5 g/cm^3 , is a significant improvement. The refinement of the size distribution of meteoroids is another significant improvement. Changes in the size distribution of meteoroids in the model were made only in the size range of the data obtained on the LDEF. The size distribution of large meteoroids was not changed, and this model would predict essentially the same meteoroid hazard to a space station, for example, as the previous model. As far as sub-micron meteoroids go, the model presented in this paper does not apply. It has a cutoff in the size of meteoroids at $1 \mu\text{m}$, just as the previous model did. Certainly sub-micron meteoroids exist, as shown by the Interplanetary Dust Experiment on the LDEF for instance, but they may very well be meteoroids of a completely different nature than those that are larger than a micron, and may need to be modelled as a separate component of the meteoroid environment. The sub-micron meteoroids may be influenced by forces that do not affect larger particles and may have a speed distribution and a directionality with respect to the Earth quite different from the larger meteoroids so that it would be inappropriate to include them in the model presented in this paper.

There is some question as to whether the anodized layer caused the craters from small meteoroids to be undersized so that the crater size distribution on the space-facing end of the LDEF does not properly reflect the size distribution of meteoroids. It may be that the small craters would have been slightly larger in a plate that was not anodized and that the size distribution of meteoroids from the NASA model (ref.1) is accurate for small meteoroids. Hypervelocity impact tests should provide insight. However, it has been assumed in this paper that the aluminum oxide layer on the one plate from the space-facing end, used to determine the size distribution of small meteoroids (plate H5), did not affect the crater size noticeably, based on the observation that that plate did not appear to have an aluminum oxide layer other than the natural oxide layer that occurs due to exposure to the atmosphere. For most of the other plates examined in this study, the aluminum oxide layer probably did affect the size of small craters, perhaps even the formation of lips on larger craters, e.g. the B9P2 and B9P4 plates. Future meteoroid studies of this nature should not use anodized plates if possible.

It was assumed that all meteoroids have the same density (2.5 g/cm^3) because no data on the distribution of meteoroid densities were available. However, there is a recent study awaiting publication in which Love (ref.16) will show that interplanetary dust particles in the 5-15 micron size range, that were captured in the stratosphere, have a distribution of densities ranging from 0.3 g/cm^3 to 6.2 g/cm^3 with a mean of 2.0 g/cm^3 . When a correction is made for the effect that

particle density has on the atmospheric fall speed, and thus on the collection rate, it was found that the mean density of meteoroids in space, just outside the atmosphere, is 2.8 g/cm^3 . This is in good agreement with the mean density assumed in this study. Future models of the near-Earth meteoroid environment should include the distribution of meteoroid densities. Of course, the density distribution may vary with particle size and additional data will be valuable.

The uncertainty in the data that results from the statistically small number of craters found on the LDEF (which is seen in the 90 percent confidence limits in the figures) is not the only uncertainty in the data. Measurement of the crater lip diameter requires judgement, and different people using different microscopes with different illumination sources will systematically differ in their measurement of crater lip diameters. A 10 percent systematic difference in the measurement of the lip diameter, which is certainly possible, can produce a difference in the reported flux of craters above a given threshold size, much greater than 10 percent, because the size distribution is such that many craters tend to be near the threshold size.

While the size distribution of meteoroids was determined from a set of craters on an LDEF face that was essentially free of man-made debris impacts, the speed distribution and directionality of meteoroids were determined from data on all the faces of the LDEF, and most were contaminated to an unknown degree by impacts from man-made debris. It can only be said that the Erickson and Kessler speed distributions and the random directionality are reasonable. Other speed distributions and directionalities could be found that are also reasonable, and those distributions could suggest either a greater or a lesser amount of man-made debris. While it would appear that meteoroids dominate the particulate environment in the $20 \text{ }\mu\text{m}$ to $200 \text{ }\mu\text{m}$ diameter size range, the extent of that domination is still uncertain.

REFERENCES

1. Meteoroid Environment Model - 1969 (Near Earth to Lunar Surface). NASA Space Vehicle Design Criteria (Environment). NASA SP-8013, 1969.
2. Meteoroid Environment Model - 1970 (Interplanetary and Planetary). NASA Space Vehicle Design Criteria (Environment). NASA SP-8038, 1970.
3. Meteoroid Damage Assessment. NASA Space Vehicle Design Criteria (Structures). NASA SP-8042, 1970.
4. Kessler, D.J.; Reynolds, R.C.; and Anz-Meador, P.D.: Orbital Debris Environment for Spacecraft Designed to Operate in Low Earth Orbit. NASA Technical Memorandum 100471, 1989.
5. Humes, D.H.: Large Craters on the Meteoroid and Space Debris Impact Experiment. LDEF - 69 Months in Space, First Post-Retrieval Symposium, NASA CP-3134, pp.399-422, 1991.
6. Peters, P.N.; Whitehouse, P.L.; and Gregory, J.C.: Refinements on the Pinhole Camera Measurements of the LDEF Attitude. LDEF - 69 Months in Space, Second Post-Retrieval Symposium, NASA CP-3194, pp.3-12, 1992.
7. Alvarez, J.M.: Statistical Analysis of Meteoroid Penetration Data Including Effects of Cutoff. NASA TN D-5668, 1970.
8. Erickson, J.E.: Velocity Distribution of Sporadic Photographic Meteors. Journal of Geophysical Research, vol.7, no.12, 3721-3726, 1968.
9. Kessler, D.J.: Average Relative Velocity of Sporadic Meteoroids in Interplanetary Space. AIAA Journal, vol.7, no.12, 2337-2338, 1969.
10. Watts, A.; Atkinson, D.; and Rioco, S.: Dimensional Scaling for Impact Cratering and Perforation. Presented at the Third LDEF Post-Retrieval Symposium, Williamsburg, VA, 1993.
11. Zook, H.A.: The State of Meteoritic Material on the Moon. Proceedings of the Sixth Lunar Science Conference, pp. 1653-1672, 1975.
12. Grün, E.; Zook, H.A.; Fechtig, H.; and Giese, R.H.: Collisional Balance of the Meteoritic Complex, Icarus, vol.62, p.244, 1985.

13. Warren, J.L.; Zook, H.A.; Allton, J.H.; Clanton, U.S.; Dardano, C.B.; Holder, J.A.; Marlow, R.R.; Schultz, R.A.; Watts, L.A.; and Wentworth, S.J.: The Detection and Observation of Meteoroid and Space Debris Impact Features on the Solar Max Satellite. Proceedings of the 19th Lunar and Planetary Science Conference, pp.641-657, 1989.
14. McKay, D.S.: Microparticle Impacts in Space - Results from Solar Max Satellite and Shuttle Witness Plate Inspections. NASA Conference Publication 3035, Part 1, pp.301-327, 1988.
15. Naumann, R.J.: The Near-Earth Meteoroid Environment. NASA TN D-3717, 1966.
16. Love, S.G.; Joswiak, D.J.; and Brownlee, D.E.: Densities of Stratospheric Micrometeorites. Submitted to Icarus 17 December 1993; revised 14 April 1994.

TABLE I. Location of the craters on the LDEF, with a lip diameter of 100 μ m or greater, considered in this paper.

Orientation	Plate	Area,m ²	Number of craters with lip diameter...				
			$\geq 100\mu\text{m}$	$\geq 200\mu\text{m}$	$\geq 300\mu\text{m}$	$\geq 500\mu\text{m}$	$\geq 1000\mu\text{m}$
8°	B9P1	.139				14	3
8°	B9P2	.183	269	106	60	24	2
8°	B9P3	.044				4	1
8°	B9P4	.117	131	51	21	6	0
8°	B9P5	.0185				0	0
8°	B9P6	.0387				2	1
8°	B9P7	.00180				1	0
8°	B9P9	.00144				0	0
8°	B9P11	.00144				0	0
8°	B9P12	.00144				0	0
8°	B9P14	.00144				0	0
8°	B9P15	.00144				0	0
8°	B9P18	.00144				0	0
8°	B9P22	.00180				0	0
8°	B9P24	.00180				0	0
8°	B9P28	.00180				0	0
8°	B9P32	.00180				0	0
8°	B9P33	.00180				0	0
8°	B9P34	.00346				0	0
8°	B9P36	.00346				0	0
8°	B9P37	.00357				0	0
8°	B9P40	.00396				0	0
8°	B9P43	.00266				0	0
8°	B9P44	.00266				0	0
8°	B9P45	.00266				0	0
8°	B9P46	.00453				0	0
8°	B9P48	.00453				0	0
8°	B9P51	.00335				0	0
8°	B9P54	.00180				0	0
8°	B9P55	.00180				0	0
8°	B9P57	.00180				0	0
8°	B9P58	.00335				0	0
8°	B9P60	.00266				0	0
8°	B9P61	.00357				0	0
8°	B9P62	.00396				0	0
8°	G22(R9)	.15				9	2
8°	H22(R9)	.15				9	5

TABLE I. Continued

<u>Orientation</u>	<u>Plate</u>	<u>Area,m²</u>	<u>Number of craters with lip diameter...</u>				
			<u>≥100μm</u>	<u>≥200μm</u>	<u>≥300μm</u>	<u>≥500μm</u>	<u>≥1000μm</u>
22°	F10G	.59				46	8
22°	F10H	.59	685	262	120	32	9
22°	G23(R10)	.15				14	2
22°	H23(R10)	.15				17	3
38°	B8G	.39	410	176	84	25	2
38°	B8H	.39	366	143	72	28	2
38°	G21(R8)	.15				7	2
38°	H21(R8)	.15				11	2
52°	B11G	.59				36	7
52°	B11H	.59				30	3
52°	E11G	.59				36	1
52°	E11H	.59				32	2
52°	F11G	.59	505	200	95	31	3
52°	F11H	.59				28	4
52°	G24(R11)	.15				3	0
52°	H24(R11)	.15				5	1
68°	C7G	.59				22	1
68°	C7H	.59				16	3
68°	E7G	.59				26	4
68°	E7H	.59				31	3
68°	F7G	.59	410	165	71	18	1
68°	F7H	.59				20	2
68°	G20(R7)	.15				6	3
82°	A12G	.59	312	107	53	17	4
82°	A12H	.59				15	0
82°	H13(R12)	.15				7	4
98°	A6G	.59				7	2
98°	A6H	.56				9	2
98°	B6G	.59	215	83	35	7	1
98°	B6H	.59				11	2
98°	D6G	.39				10	1
98°	D6H	.39				11	0
98°	H19(R6)	.15				5	1

TABLE I. Continued

<u>Orientation</u>	<u>Plate</u>	<u>Area,m²</u>	Number of craters with lip diameter...				
			<u>≥100μm</u>	<u>≥200μm</u>	<u>≥300μm</u>	<u>≥500μm</u>	<u>≥1000μm</u>
112°	B1G	.59				12	1
112°	B1H	.59				5	0
112°	E1G	.59				18	1
112°	E1H	.59				8	0
112°	F1G	.59	141	44	18	2	0
112°	F1H	.59				8	0
112°	G14(R1)	.15				3	0
112°	H14(R1)	.15				2	0
128°	A5G	.59				5	0
128°	A5H	.59				2	1
128°	F5G	.59	86	31	16	5	1
128°	F5H	.59				2	1
128°	G18(R5)	.15				0	0
128°	H18(R5)	.15				2	0
142°	B2G	.59	70	30	19	3	1
142°	B2H	.59				2	0
142°	D2G	.39				1	0
142°	D2H	.39				2	0
142°	G15(R2)	.15				0	0
142°	H15(R2)	.15				3	0
158°	C4G	.59	56	17	8	0	0
158°	C4H	.59				4	0
158°	E4G	.59				3	0
158°	E4H	.59				4	1
158°	G17(R4)	.15				2	1
158°	H17(R4)	.15				1	0
172°	F3G	.59	48	20	13	5	1
172°	F3H	.59				3	1
172°	G16(R3)	.15				0	0
172°	H16(R3)	.15				2	1

TABLE I. Concluded

<u>Orientation</u>	<u>Plate</u>	<u>Area,m²</u>	<u>Number of craters with lip diameter...</u>				
			<u>≥100μm</u>	<u>≥200μm</u>	<u>≥300μm</u>	<u>≥500μm</u>	<u>≥1000μm</u>
Earth	G3	.90				0	0
Earth	G4	.52	9	3	2	1	0
Earth	G8	.52				0	0
Earth	G9	.90				0	0
Earth	G13(E)	.63				1	0
Earth	G14(E)	.35	3	1	1	1	1
Earth	G15(E)	.35				0	0
Earth	G16(E)	.63				0	0
Earth	G17(E)	.35				0	0
Earth	G18(E)	.35				0	0
Earth	G19(E)	.63				0	0
Earth	G20(E)	.35	2	2	1	1	0
Earth	G21(E)	.35				0	0
Earth	G22(E)	.63				0	0
Earth	G23(E)	.35				0	0
Earth	G24(E)	.35				0	0
Space	H5	.52	275	100	56	20	1
Space	H13(S)	.63				19	2
Space	H14(S)	.35				8	1
Space	H15(S)	.35				6	0
Space	H16(S)	.63				21	1
Space	H17(S)	.35				4	0
Space	H18(S)	.35				12	1
Space	H19(S)	.62	348	113	61	23	2
Space	H21(S)	.35				7	1
Space	H22(S)	.63				24	5
Space	H23(S)	.35				8	0
Space	H24(S)	.35				12	3

TABLE II. Location of the craters on the LDEF, with a lip diameter less than 100 μ m, considered in this paper.

<u>Orientation</u>	<u>Plate</u>	<u>Area,m²</u>	<u>$\geq 10\mu\text{m}$</u>	<u>$\geq 20\mu\text{m}$</u>	<u>$\geq 30\mu\text{m}$</u>	<u>$\geq 40\mu\text{m}$</u>	<u>$\geq 60\mu\text{m}$</u>	<u>$\geq 80\mu\text{m}$</u>
Space	H5	.52					468 *	338
Space	H19(S)	.62					638 *	453
Space	H5 ^c	.0447	189 **	141	107	78	51	36

c Square area at center of H5 plate scanned at high power - 1 mm field of view

* Not expected to be a complete count - 14 mm field of view

** Not expected to be a complete count - 1 mm field of view

TABLE III. Material properties of aluminum alloys.

<u>Alloy</u>	<u>Density</u> $\rho_t, (\text{kg m}^{-3})$	<u>Sound Speed</u> $c_t, (\text{m s}^{-1})$	<u>Typical Yield Strength</u> $Y_t, (\text{N m}^{-2})$	<u>Typical Ultimate Strength</u> $\sigma_s, (\text{N m}^{-2})$	<u>Stress Factor</u> s	<u>Grain Size Parameter</u> $\Delta, (\text{m})$
1145-H19	≈ 2700	≈ 5100	1.31×10^8	1.45×10^8	1.50	?
2024-T3	2770	5100	3.45×10^8	4.83×10^8	1.60	?
6061-T6	2700	5100	2.76×10^8	3.10×10^8	1.42	50×10^{-6}

TABLE IV. Number of craters of various sizes in the aluminum louvers on the Solar Max spacecraft (ref.13).

Lip Diameter, μm	≥ 40	≥ 60	≥ 80	≥ 100	≥ 120	≥ 160
Number*	436	267	196	153	120	86
Flux, raw, $\text{m}^{-2}\text{s}^{-1}$	5.74E-6	3.51E-6	2.58E-6	2.01E-6	1.58E-6	1.13E-6
Flux, unshielded, $\text{m}^{-2}\text{s}^{-1}$	8.08E-6	4.94E-6	3.63E-6	2.83E-6	2.23E-6	1.59E-6

* Craters and holes, because holes would be big craters in a thick plate.

Area = 0.5800 m^2 (use this, not reduced area, because number of features on the reduced area is not known and there is no reason to use the reduced area for crater analysis.

Time = 1517 days

Transmission factor, which is the fraction of the viewing sphere around the detectors that is not shielded by other spacecraft components, is 0.71.

TABLE V. Penetration data from spacecraft in low-Earth orbit.

Spacecraft				Detector				Data			
Name	Years of operation	Inclination	Altitude, km	Material	Thickness, μm	Area, m^2	Transmission factor \dagger	Penetrations	Duration, days	Unshielded flux, $\text{m}^{-2}\text{s}^{-1}$	Source
Explorer 16	1962-1963	52°	750-1180	Beryllium-copper	25	1.41*	.70	44	200	3.9×10^{-6}	Ref. 7
Explorer 16	1962-1963	52°	750-1180	Beryllium-copper	51	0.564*	.70	11	200	2.0×10^{-6}	Ref. 7
Explorer 23	1964-1965	52°	458-1000	Stainless steel	25	0.987*	.70	50	370	4.4×10^{-6}	Ref. 7
Explorer 23	1964-1965	52°	458-1000	Stainless steel	51	1.974*	.70	74	370	2.5×10^{-6}	Ref. 7
Pegasus 1,2,3	1965-1966	28.9°-31.8°	496-748	Aluminum + mylar	38 + 13	≈ 8	1.00	582	—	2.2×10^{-6}	Ref. 15
Pegasus 1,2,3	1965-1966	28.9°-31.8°	496-748	Aluminum + mylar	200 + 13	≈ 17	1.00	49	—	2.4×10^{-7}	Ref. 15
Pegasus 1,2,3	1965-1966	28.9°-31.8°	496-748	Aluminum + mylar	400 + 13	≈ 175	1.00	201	—	5.6×10^{-8}	Ref. 15
Solar Max	1980-1984	28.5°	500-570	Kapton	50	1.64	0.55	370	1517	3.1×10^{-6}	Ref. 13
Solar Max	1980-1984	28.5°	500-570	Kapton	75	0.207	0.98	57	1517	2.1×10^{-6}	Ref. 13
Solar Max	1980-1984	28.5°	500-570	Aluminum	125	0.8904	0.71	65	1517	7.8×10^{-7}	Ref. 13

* Area decreases with each cell penetrated

\dagger Transmission factor is the fraction of the viewing sphere around the detectors that is not shielded by other spacecraft components

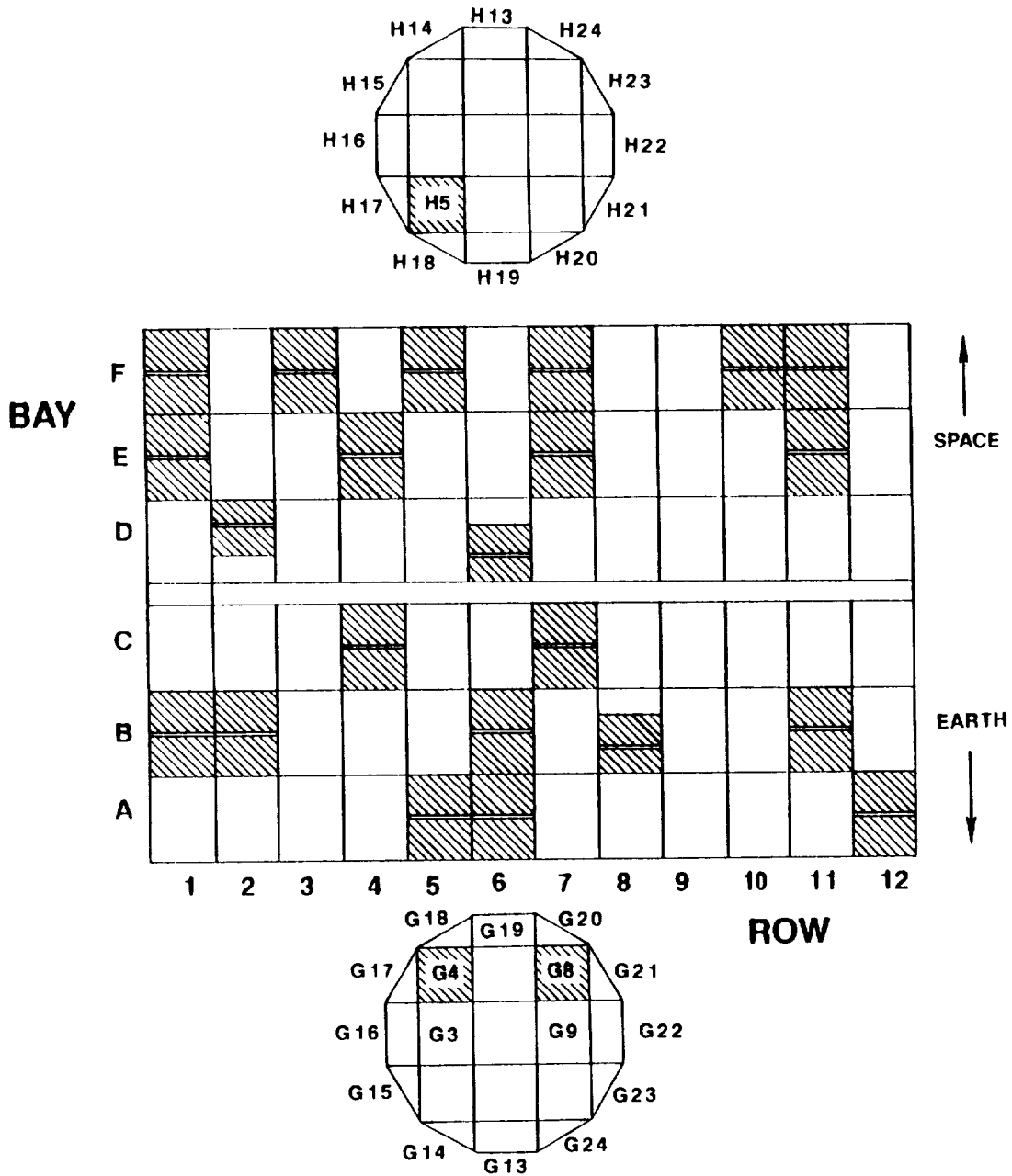


Fig. 1. Identification system used for the tray locations and the thermal panels on the LDEF. The shaded areas show the location of the Meteoroid and Space Debris Impact Experiment plates. The location of the dummy plates used in this study is also shown.

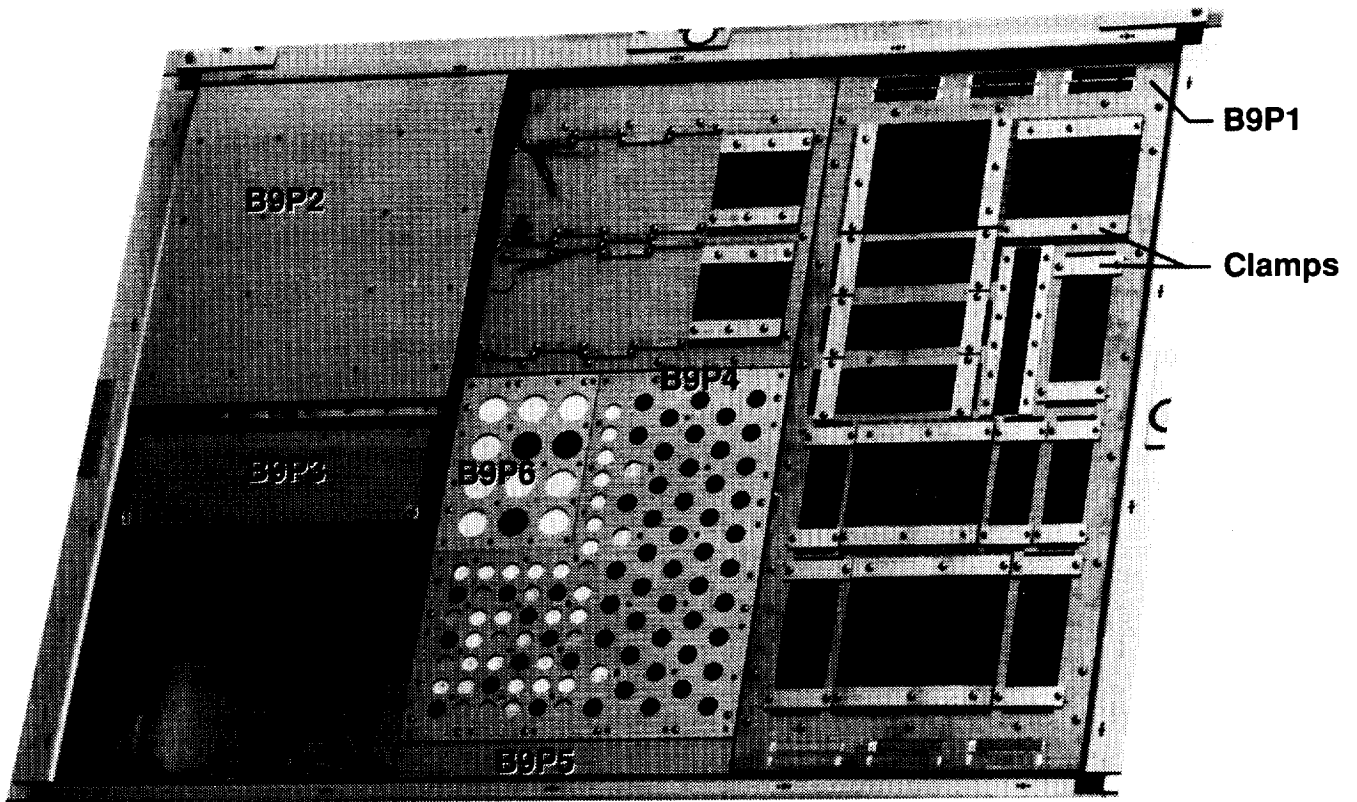


Fig. 2. Tray B9 containing aluminum plates and clamps donated by Wayne Slempt to the LDEF M&D SIG that were examined in this study.

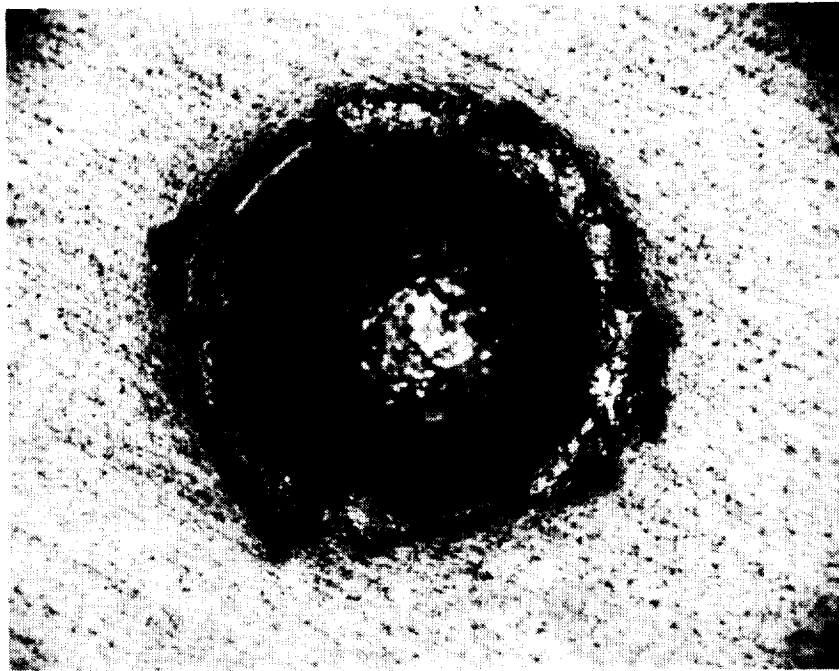


Fig. 3. Largest crater on the Meteoroid and Space Debris Impact Experiment. A 4 mm diameter crater on plate F10H.

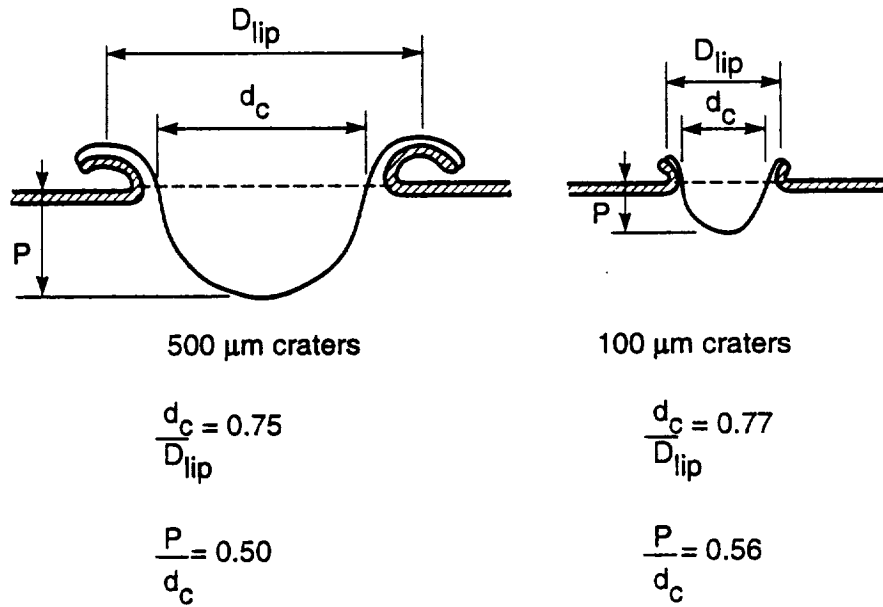


Fig. 4. Typical shapes of craters in aluminum alloy 6061-T6 on the LDEF.

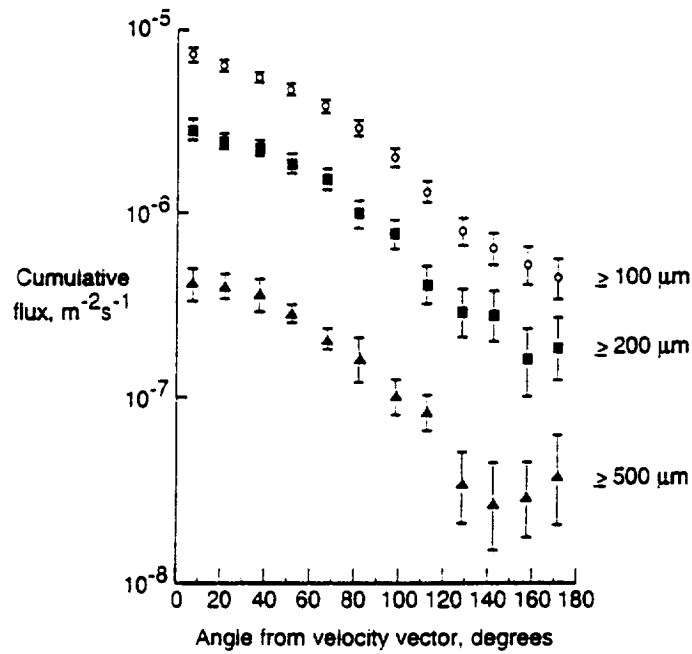


Fig. 5. Measured cumulative crater flux on the twelve peripheral rows around the LDEF, for craters with threshold lip diameters of 0.1 mm, 0.2 mm, and 0.5 mm.

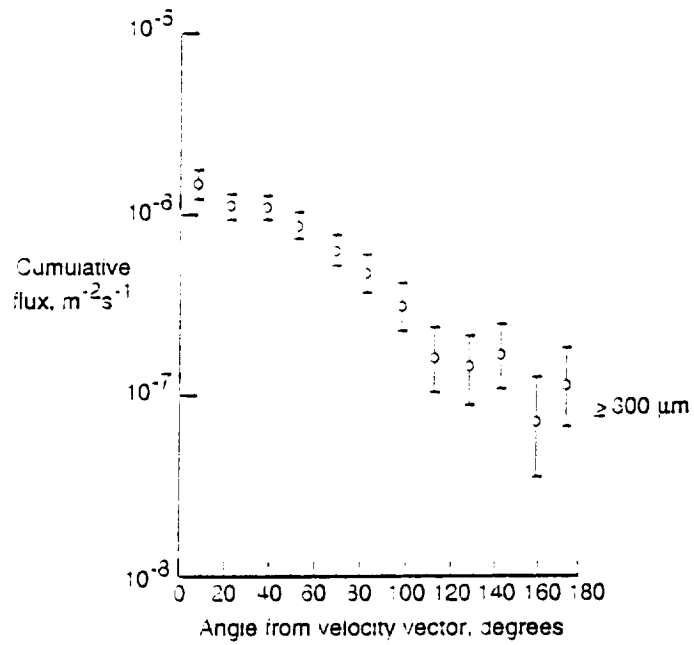


Fig. 6. Measured cumulative crater flux on the twelve peripheral rows around the LDEF, for craters with a threshold lip diameter of 0.3 mm.

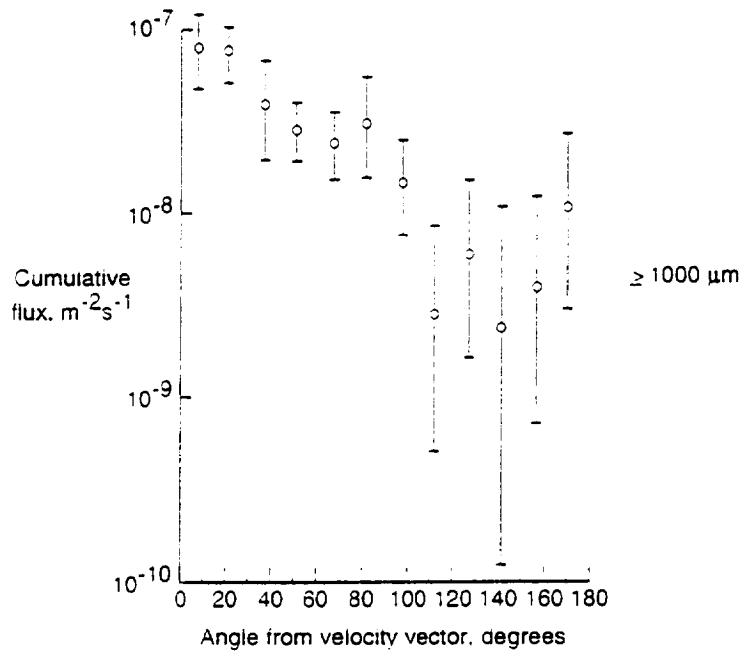


Fig. 7. Measured cumulative crater flux on the twelve peripheral rows around the LDEF, for craters with a threshold lip diameter of 1 mm.

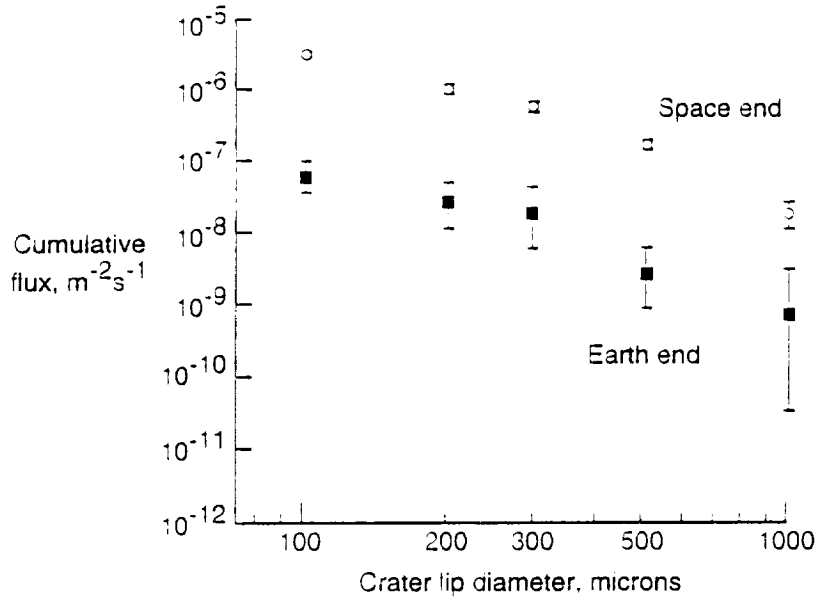


Fig. 8. Measured cumulative crater flux on the two ends of the LDEF, for craters with threshold lip diameters in the 0.1 mm to 1 mm range.

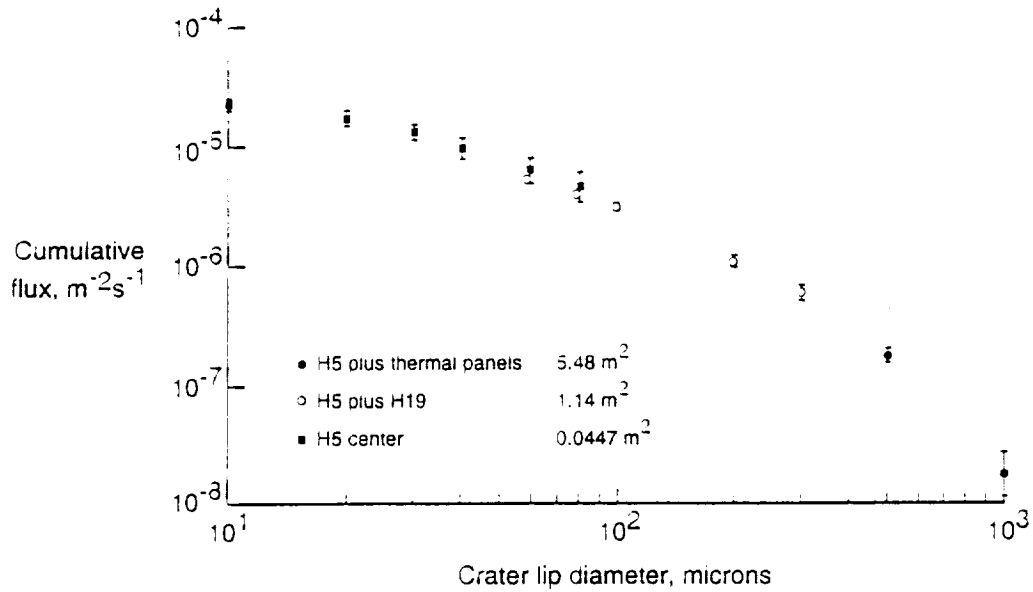


Fig. 9. Measured cumulative crater flux on the space-facing end of the LDEF, for craters with threshold lip diameters in the 10 μ m to 1 mm range.

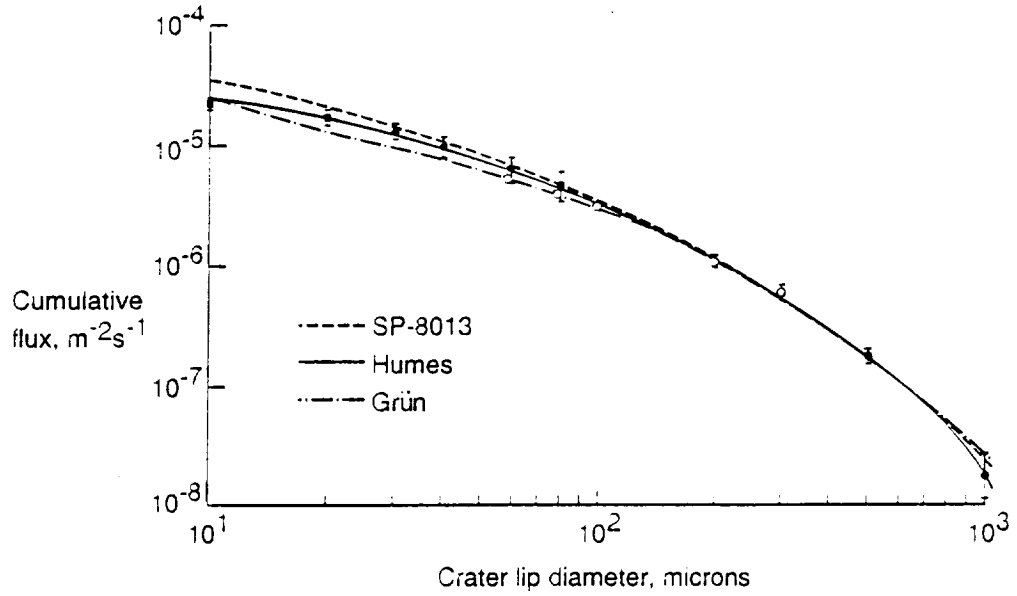


Fig. 10. Calculated cumulative meteoroid crater flux on the space-facing end of the LDEF, for craters with threshold lip diameters in the 10 μm to 1 mm range, compared to the measured crater fluxes.

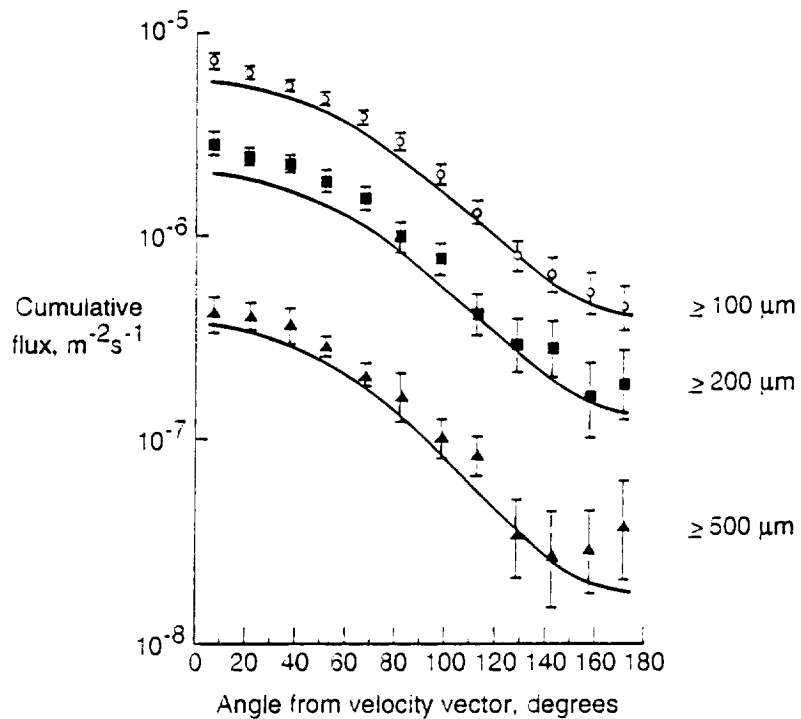


Fig. 11. Calculated cumulative meteoroid crater flux on the twelve peripheral rows around the LDEF, for craters with threshold lip diameters of 0.1 mm, 0.2 mm, and 0.5 mm, compared to the measured crater fluxes.

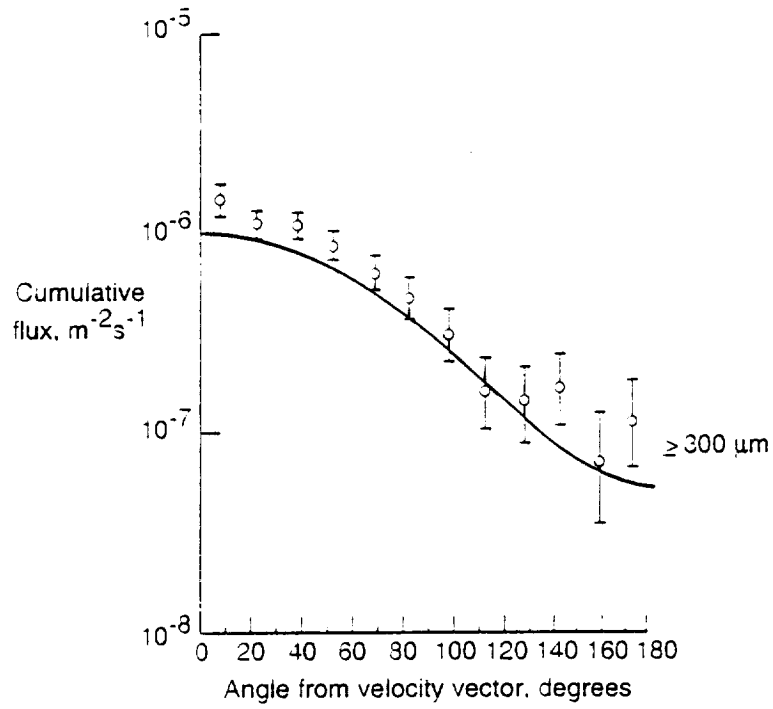


Fig. 12. Calculated cumulative meteoroid crater flux on the twelve peripheral rows around the LDEF, for craters with a threshold lip diameter of 0.3 mm, compared to the measured crater fluxes.

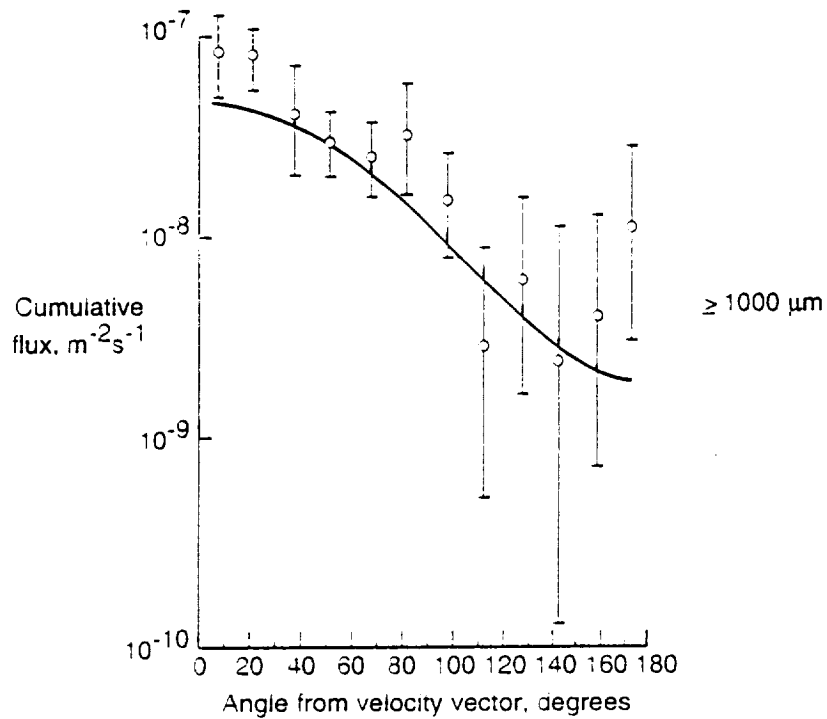


Fig. 13. Calculated cumulative meteoroid crater flux on the twelve peripheral rows around the LDEF, for craters with a threshold lip diameter of 1 mm, compared to the measured crater fluxes.

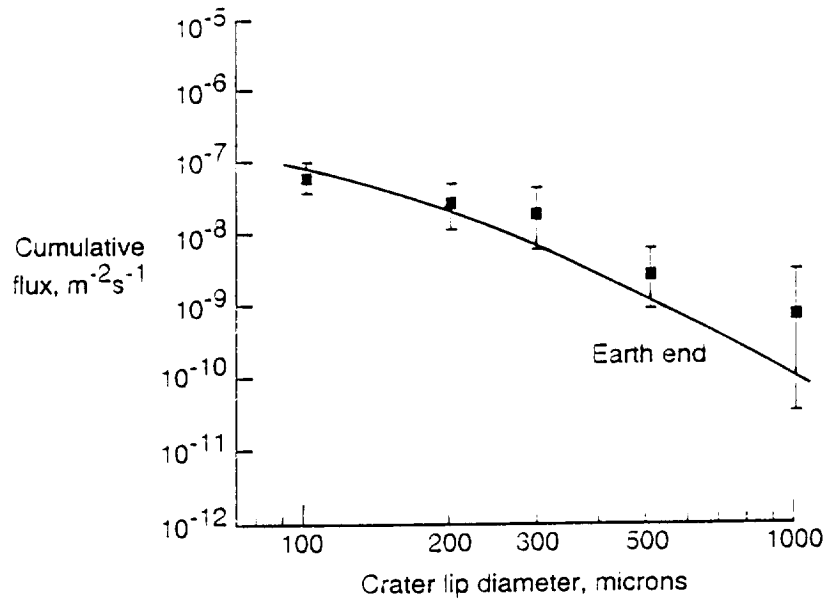


Fig. 14. Calculated cumulative meteoroid crater flux on the Earth-facing end of the LDEF, for craters with threshold lip diameters in the 0.1 mm to 1 mm size range, compared to the measured fluxes.

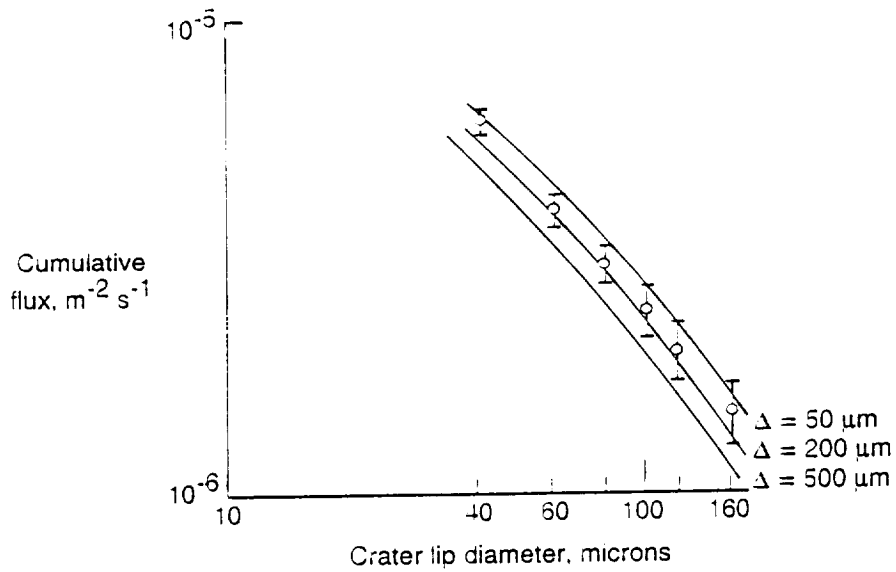


Fig. 15. Calculated cumulative meteoroid crater flux on the aluminum louvers from the Solar Max spacecraft, compared to the measured fluxes.

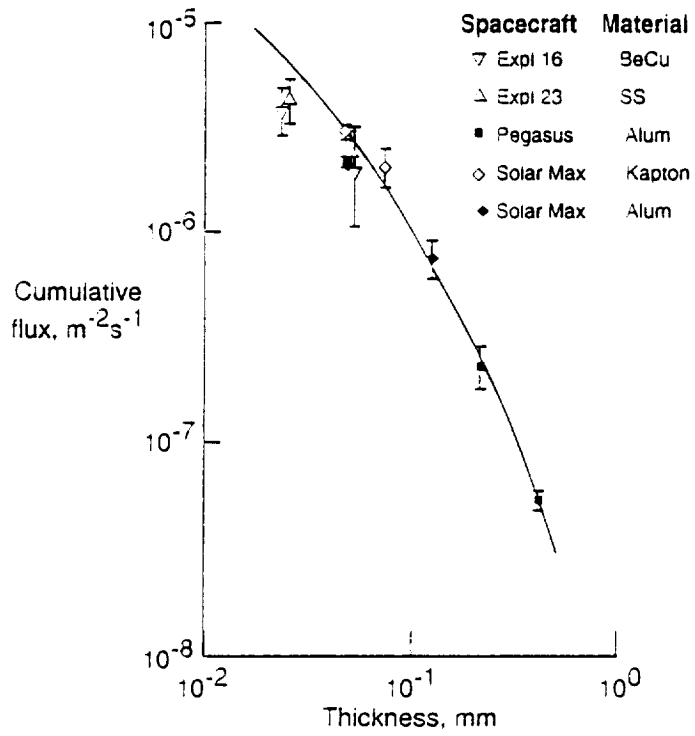


Fig. 16. Calculated meteoroid penetration flux for an unshielded aluminum (2024-T4) plate at an altitude of 700 km, compared to the penetration data for various materials from the Explorer 16, Explorer 23, and the three Pegasus spacecraft. The filled symbols are for aluminum detectors.